PAPER

Check for updates

Enhanced protein synthesis from immobilized circular DNA *via* triple-helix formation

Shunsuke Takahashi, [ID] *[a] Kazuki Hayashi,[b] Jun Okada,[b] Hibiki Takashima,[b] Koko Nakata,[a] Masahiko Oshige*[b,c] and Shinji Katsura*[b,c]

Efficient immobilization of DNA on solid surfaces is important for the advancement of electrochemical DNA sensors, biosensors, and bioelectrodes. In this study, we established a new method for immobilizing circular DNA through the formation of triple-helical structures, enabling the high-density and oriented attachment of plasmid DNA to the substrate surface. We engineered biotinylated circular DNA containing a triple-stranded region by hybridizing a biotinylated homopyrimidine third strand with homopurine–homopyrimidine sequences in circular DNA. Subsequently, the modified circular DNA was effectively immobilized on a streptavidin–biotin-functionalized substrate. Using a cell-free protein synthesis system, the yield of *Discosoma* sp. red (DsRed) fluorescent protein synthesized from immobilized circular DNA was approximately 4.6 times higher than that from immobilized linear DNA. Notably, the immobilized circular DNA template was effectively reused in multiple consecutive rounds of protein synthesis, highlighting its potential for repeated application. Overall, our strategy significantly enhances protein synthesis efficiency and provides a robust platform for the development of high-performance DNA arrays, biosensors, and bioelectrodes.

1. Introduction

Solid-phase assay systems are indispensable tools for the detection of a wide range of analytes, from small molecules to complex biomolecules such as DNA and proteins, in modern analytical science.[1–3] A key aspect of these systems is the immobilization of biomolecules on solid surfaces, which is fundamental for developing DNA arrays, protein arrays, biosensors, and bioelectrodes for various analytical and bioelectronic applications.[4–7] DNA arrays (DNA microarrays) have revolutionized genomics by enabling the high-throughput analysis of gene expression and genetic variation.[8,9] Similarly, protein arrays are powerful tools in proteomics for the simultaneous detection and quantification of multiple proteins.[10,11] However, the performance of these array-based platforms strongly depends on the immobilization method used, which directly influences the stability, activity, and accessibility of immobilized biomolecules.

[a]Division of Life Science and Engineering, School of Science and Engineering, Tokyo Denki University, Ishizaka, Hatoyama-cho, Hiki-gun, Saitama350-0394, Japan. E-mail: stakahashi@mail.dendai.ac.jp
[b]Department of Environmental Engineering Science, Graduate School of Science and Technology, Gunma University, Kiryu, Gunma 376-8515, Japan. E-mail: oshige@gunma-u.ac.jp, katsura@gunma-u.ac.jp
[c]Gunma University Center for Food Science and Wellness (GUCFW), Aramaki, Gunma 371-8510, Japan

Various techniques have been developed for efficient DNA immobilization on surfaces. Physical adsorption methods rely on electrostatic interactions between negatively charged DNA and positively charged surface coatings such as poly L-lysine,[12] polypyrrole,[13] polyaniline,[14] and polyethyleneimine.[15] Chemisorption involves the formation of covalent bonds between thiol- or amine-modified DNA and metal surfaces or specific functional groups on substrates.[16–19] Affinity-based approaches use biotin- or digoxigenin-labeled DNA immobilized on surfaces modified with avidin–biotin or anti-digoxigenin systems.[20,21] These methods can immobilize large amounts of DNA at high surface densities; however, controlling the orientation of the immobilized DNA remains a significant challenge. Proper orientation is essential to ensure that immobilized DNA strands are accessible for hybridization with complementary targets and binding interactions with DNA-binding proteins.

Single-stranded oligonucleotides and double-stranded DNA fragments have been extensively used as immobilization probes owing to their ease of synthesis and modification.[12–23] However, immobilized linear DNA has several limitations. Linear DNA strands are susceptible to degradation by exonucleases and cannot form supercoiled structures, which restricts their stability and transcriptional function in biological assays. These issues can reduce the efficiency of downstream applications, such as *in vitro* transcription, translation, and hybridization.

To address the limitations of linear DNA immobilization and enhance protein expression efficiency, we focused on covalently immobilizing circular DNA on substrate surfaces. Circular DNA exhibits distinct advantages, such as resistance to exonuclease digestion and the ability to form supercoiled conformations that enhance transcriptional activity.[24,25] The formation of a DNA triple-helix structure is a promising strategy for immobilizing circular DNA in a controlled orientation. In this method, a homopyrimidine (Py) or homopurine (Pu) third strand is hybridized into the major groove of a homopurine–homopyrimidine (Pu–Py) sequence in the Watson–Crick duplex *via* Hoogsteen hydrogen bonds.[26] The third strand binds in parallel to the purine-rich strand of the duplex DNA. However, the efficient formation of triple-helical structures generally requires acidic conditions (pH ≤ 6) because of the need for hemi-protonated cytosine residues.[27] The structures and energetics of DNA triplexes have been extensively studied,[28,29] providing a foundation for their application in DNA-immobilization.

In our strategy, a biotinylated homopyrimidine oligonucleotide (third strand) was hybridized with a complementary PuPy sequence engineered into a circular DNA plasmid, generating a biotinylated circular DNA containing a stable triplex region. The biotinylated triple-helix region enabled the circular DNA to be captured on a streptavidin–biotin-modified surface in an oriented manner (anchored *via* the biotinylated site). Using a cell-free protein synthesis system, we demonstrated that genes encoded on the immobilized circular DNA are efficiently transcribed and translated into proteins. In this study, the monomeric form of the *Discosoma* sp. red fluorescent protein (DsRed) was selected as a model because of its advantageous properties. Specifically, monomeric DsRed avoids oligomerization and matures rapidly, thereby providing a bright and reproducible luminescence signal that is ideal for cell-free protein synthesis.[30,31] The amount of DsRed produced from immobilized circular DNA was approximately 4.6 times higher than that produced from immobilized linear DNA. Furthermore, the immobilized circular DNA template could be reused for multiple protein synthesis cycles with measurable output, highlighting the potential of this approach for reusable, high-density DNA templates in biosensing and bioengineering applications.

2. Experimental

2.1 Materials

L-Cysteine was purchased from Tokyo Chemical Industry (Tokyo, Japan). Biotin-(AC$_5$)$_2$ sulfo-OSu (6-[6-(biotinylamino) hexanoylamino] hexanoic acid *N*-hydroxysulfosuccinimide ester) was obtained from Dojindo (Kumamoto, Japan). Chemically synthesized single-stranded oligonucleotides were obtained from Japan Bio Services (Saitama, Japan). Restriction enzymes Bst1107 I, BamHI, and HindIII were purchased from TaKaRa Bio, Inc. (Tokyo, Japan). Phusion High-Fidelity DNA Polymerase was obtained from Thermo Fisher Scientific

(Waltham, MA, USA). All other reagents were of analytical grade and purchased from Sigma-Aldrich (St Louis, MO, USA), Nacalai Tesque (Kyoto, Japan), and FUJIFILM Wako Pure Chemical Corporation (Osaka, Japan).

2.2 Construction of circular DNA with triple helix forming sequence

The plasmid pUC19 containing a homopyrimidine–homopurine (PyPu) sequence insert (pUC19-PyPu) was a kind gift from Ms. Y. Morii (Toyohashi University of Technology, Japan).[26] A DNA fragment containing the designed PyPu sequence was synthesized by PCR using the primers 5′-AATTTCTTTTCT TTTTCTTTTCTCGAG-3′ and 5′-AGCTCTCGAGAAAAGAAAAAGA AAAGA-3′. The resulting DNA fragment was inserted into the pUC19 plasmid, which was digested with BamHI and HindIII using the DNA Ligation Kit Mighty Mix (TaKaRa Bio), yielding the plasmid pUC19-PyPu (Fig. S1). The construct was transformed into *Escherichia coli* XL1-Blue competent cells (Agilent Technologies). Positive transformants were selected, and plasmid DNA was purified from a 100 mL culture using a Qiagen Plasmid Midi Kit (Qiagen). The resulting DNA concentration was measured using a UV-Vis spectrophotometer (UVmini-1240; Shimadzu, Kyoto, Japan).

2.3 Construction of DsRed expression plasmid with a triple helix forming sequence

The PyPu sequence from pUC19-PyPu was amplified by PCR using the primers 5′-CGATAGCGGAGTGTACGGCATCAGAGCA GATTGTA-3′ and 5′-ATAGTTAAGCCAGTAGAGTCAGTGAGCGAG GAAGC-3′. The PCR product containing the PyPu triple-helix target sequence was cloned into the pET21a vector at the Bst1107 I restriction site using an In-Fusion cloning kit (TaKaRa Bio), yielding pET21a-PyPu.

Separately, the gene encoding DsRed fluorescent protein (from plasmid pDsRed-Monomer, TaKaRa Bio) was PCR-amplified with the forward primer 5′-CGCGGATCCGCGATGGAC AACACCGAGGACGTC-3′ and reverse primer 5′-CCCAAGCTTG GGCTGGGAGCCGGAGTGGCG-3′. The DsRed PCR product was digested with BamHI and HindIII and ligated into pET21a-PyPu using the DNA Ligation Kit Mighty Mix, yielding the expression plasmid, pET21a-PyPu-DsRed (Fig. 1 and S1). The ligation product was transformed into *E. coli* XL1-Blue cells, and the plasmid DNA was purified as described previously. The DNA concentration was measured spectrophotometrically.

2.4 Assay for triple-helix formation

To prepare DNA fragments for triple helix formation, pUC19-PyPu plasmid DNA was digested with PvuII and XhoI. The resulting DNA fragments were purified by ethanol precipitation, and their concentrations were determined using a UV-Vis spectrophotometer (UVmini-1240; Shimadzu, Kyoto, Japan). For triple-helix formation in a 135 bp fragment containing a PuPy sequence, a 10 μL reaction mixture was prepared containing 1.5 pmol digested DNA, 10 pmol biotinylated homopyrimidine single-stranded oligonucleotide (third strand), 20 mM sodium acetate buffer (pH 5.0), and 10 mM
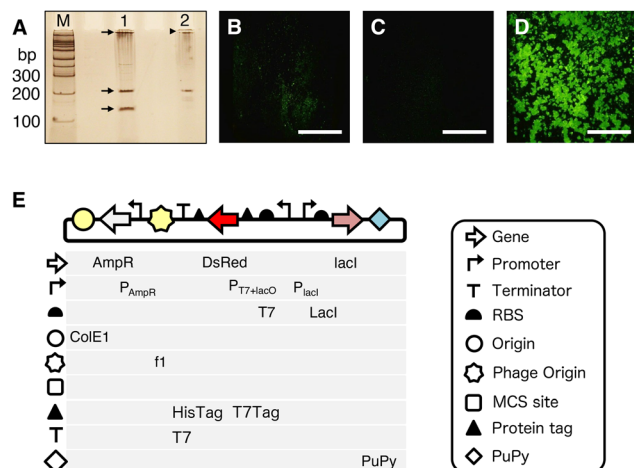
Fig. 1 (A) Electrophoretic mobility shift assay confirming triple-helix formation. A biotinylated homopyrimidine single-stranded oligo-nucleotide (third strand) was hybridized to the PuPy sequence in pUC19-PyPu to form a triple-helix structure. Arrows indicate DNA fragments of approximately 135, 200, and 5000 bp. The arrowhead indicates the upward-shifted band, which is formed by approximately 135 bp DNA fragment forming a triple helix with a biotinylated oligonucleotide and then binding to streptavidin. The samples were separated on a 12% native PAGE gel and stained using an EzStain Silver Kit. Fluorescence images of DNA immobilized on streptavidin–biotin-modified substrates under three experimental conditions: (B) unlabelled circular DNA (pET21a-PyPu-DsRed), (C) biotinylated single-stranded oligonucleotides functioning as a third strand, and (D) biotinylated circular DNA containing a triple-stranded DNA region. Following immobilization, the substrates were stained with SYBR Green I and visualized using fluorescence microscopy. The enhanced fluorescence intensity observed in (D) confirms the successful formation of the triple-helix structure. Scale bar = 1 mm. (E) plasmid maps of pET21a-PuPy-DsRed.

$MgCl_2$. The mixture was incubated at 15 °C for 3 h to form a triple helix structure. Then, 6 μL of 10 mg mL^{-1} streptavidin was added and mixed at room temperature for 10 min to bind the biotinylated triple-helix DNA to the streptavidin. Triple-helix formation was analyzed using an electrophoretic mobility shift assay (EMSA) on a 12% native polyacrylamide gel. After electrophoresis, the gel was stained with an EzStain Silver Kit (Atto, Tokyo, Japan) according to the manufacturer's instructions.

2.5 Formation of triple helix structure in circular DNA

To form a triple-helix region within pET21a-PyPu-DsRed, a 10 μL reaction containing 20 mM acetate buffer (pH 5.0), 10 mM MgCl2, 2.0 pmol of pET21a-PyPu-DsRed, and 10 pmol of a biotinylated homopyrimidine oligonucleotide (5′-AGCTCCCTTTTCTTTTTTCTTTTCT-Biotin-3′) was incubated at 15 °C for 3 h. Under these conditions, the biotinylated Py strand hybridized to the target PuPy sequence in the plasmid, forming a local triple helix with a biotin tag.

2.6 Preparation of avidin–biotin modified substrates

Gold-coated glass coverslips were used as the substrates. A thin gold film (Nilaco, Tokyo, Japan) was attached to a clean

glass coverslip (Matsunami Glass, Tokyo, Japan). The gold-coated slides were cleaned by immersion in 1.0 N nitric acid for 1 h, followed by thorough rinsing with Milli-Q water. Next, a self-assembled monolayer was formed by electrodeposition of L-cysteine: the gold-coated coverslip (working electrode, positive) and an aluminum plate (counter electrode, negative) were immersed in 10 mL of 1.0 M L-cysteine solution (pH 9.4, adjusted with NaOH). A constant current of 50 mA was applied for 5 min at 37 °C with stirring. After electrodeposition, the substrate was rinsed with Milli-Q water.

To functionalize the surface with biotin, the L-cysteine-modified gold coverslips were incubated overnight at room temperature in 7.5 mg mL^{-1} Biotin-$(AC_5)_2$ sulfo-OSu (in 50 mM $NaHCO_3$–NaOH buffer, pH 8.6). The biotinylated substrates were rinsed thoroughly with water and incubated with 5 mg mL^{-1} streptavidin in 10 mM HEPES buffer (pH 8.0) for 1 h at room temperature. After streptavidin attachment, the substrates were rinsed with water to remove unbound proteins, yielding a streptavidin–biotin-functionalized surface for DNA capture.

2.7 Immobilization of circular DNA on the prepared substrate

Circular DNA containing the biotinylated triple-helix region was spotted onto a streptavidin–biotin-modified gold substrate. The substrate was kept in a humidified chamber at room temperature for 1 h to allow the biotinylated DNA to bind to the surface via streptavidin. After incubation, the substrate was gently rinsed with Milli-Q water to remove any unbound DNA. To visualize the immobilized DNA, the surface was stained by applying 10 μL of 1× SYBR Green I nucleic acid stain (TaKaRa Bio) and incubated in the dark for 30 min. The substrate was then rinsed with water and washed briefly with 1% Triton X-100 (to reduce nonspecific background fluorescence), followed by a final water rinse. The substrate was kept wet until imaging to avoid drying artifacts from occurring.

2.8 Cell-free protein synthesis on immobilized circular DNA

The DNA-immobilized substrate prepared above was directly used as a template for in situ cell-free protein synthesis. A cell-free protein synthesis mixture was prepared according to the manufacturer's instructions (S30 T7 High-Yield Protein Expression System; Promega, Madison, WI, USA). Twenty microliters of the cell-free reaction mix was applied to the DNA-immobilized area of the substrate (ensuring that the entire spotted DNA region was covered). The substrate with the reaction mixture was incubated at 37 °C for 8 h in a humidified, sealed environment to prevent evaporation. During incubation, the setup was protected from light to minimize the photobleaching of the fluorescent protein product.

2.9 Cell-free protein synthesis on immobilized linear DNA

For comparison, a biotinylated linear DNA template encoding DsRed was also prepared. A linear DNA fragment containing a T7 promoter, DsRed coding sequence, and T7 terminator was

Therefore, the developed triple-helix-based method efficiently immobilizes circular DNA in a high-density and oriented manner on the substrate surface, providing a robust platform for downstream applications.

3.2 Enhanced cell-free protein synthesis using immobilized circular DNA

Next, we investigated whether the immobilized circular DNA could serve as an effective template for protein synthesis using a cell-free system. Using immobilized circular DNA encoding DsRed, we performed cell-free protein synthesis and monitored DsRed protein expression over time using fluorescence imaging. Fig. 2A–D shows fluorescence images of DsRed on the substrate after 0, 4, 8, and 16 h of incubation. At 0 h (Fig. 2A), a red fluorescence signal was not observed on the substrate. At 4 h (Fig. 2B), a moderate red fluorescence signal was observed on the substrate, indicating the initiation of DsRed protein synthesis. At 8 h (Fig. 2C), the fluorescence intensity was significantly increased, reflecting the robust accumulation of DsRed protein. However, only a slight increase in fluorescence intensity was observed after extending the incubation to 16 h (Fig. 2D) compared to that at 8 h. Quantitative image analysis (Fig. 2E) revealed that the amount of synthesized DsRed was approximately 39.7 ng mm^{-2} at 4 h, 61.8 ng mm^{-2} at 8 h, and 64.5 ng mm^{-2} at 16 h. The protein yield showed no statistically significant increase between 8 h and 16 h ($p < 0.01$ between 4 h and 8 h), suggesting that DsRed synthesis plateaued at approximately 8 h. This behavior is similar to that reported previously by Arce *et al.*, indicating that sfGFP expression in the S30 T7 high-yield protein expression system reaches a plateau in approximately 8 h.[32] Thus, 8 h of incubation was deemed optimal for maximal protein production in our system.

We then compared the protein expression efficiency of our immobilized circular DNA template with two other conditions: an immobilized linear DNA template and a negative control without immobilized DNA. Fluorescence images after 8 h of incubation are shown in Fig. 3A–D. Negative controls (Fig. 3A) showed no detectable fluorescence, confirming that any background or nonspecific DNA adsorption did not produce proteins on the substrate. The substrate with immobilized linear DNA (Fig. 3B) showed a fluorescent signal, indicating that
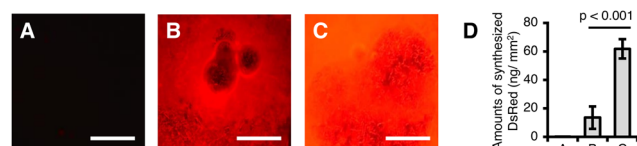

Fig. 3 Fluorescence images and yields of DsRed protein synthesized using a cell-free protein synthesis system under three DNA template conditions: (A) negative control (no immobilized DNA), (B) immobilized linear DNA, and (C) immobilized circular DNA. (D) Quantitative comparison of DsRed production using (A) non-immobilized DNA, (B) immobilized linear DNA, and (C) immobilized circular DNA. Fluorescence intensity was measured using ImageJ software. Statistical significance was determined using the *t*-test ($p < 0.001$). Error bars represent the standard deviation of three independent experiments ($n = 3$). Scale bar = 1 mm.

some DsRed was expressed from the linear template. However, the fluorescence intensity of the linear DNA template was notably lower than that of the circular DNA template (Fig. 3C). Quantitative analysis (Fig. 3D) revealed that the amount of DsRed synthesized from immobilized linear DNA was approximately 12.7 ng mm^{-2}, whereas that synthesized from immobilized circular DNA was approximately 61.8 ng mm^{-2}, indicating a significant 4.6-fold increase in protein synthesis using the immobilized circular DNA ($p < 0.001$). Although the amount of DsRed synthesized from free linear DNA templates was not evaluated in this study, our results show that the amount of DsRed synthesized from circular DNA immobilization is significantly higher than that from linear DNA immobilization in cell-free protein synthesis.

The enhanced protein synthesis from immobilized circular DNA (compared to that from immobilized linear DNA) can be attributed to several factors, as discussed below. First, linear DNA is susceptible to exonuclease degradation in cell-free systems, particularly because a linear DNA molecule presents free ends that can be attacked by the exonucleases. As an exception, enhanced protein yields from linear DNA templates in cell-free protein synthesis systems have been achieved using several strategies.[33] These include the deletion of RecBCD,[34] endA,[35] or RNase E[36] genes in *E. coli*, protection of linear DNA template ends,[37,38] and optimization of the cell-free reaction buffer.[34] However, we focused on the method of DNA immobilization in this study, whether linear or circular, and consequently, we did not implement these measures. In contrast, covalently closed circular DNA has no free ends, rendering it much more resistant to exonuclease activity and allowing it to maintain its integrity as a template throughout the reaction. Second, circular DNA can adopt supercoiled conformations, which significantly enhances its transcriptional activity.[39,40] Supercoiling induces local unwinding of the DNA helix, facilitating the initiation and elongation of transcription. In contrast, biotinylation was applied at the 5′ end of our linear DNA template, resulting in the immobilization of one end of the DNA on the surface. Immobilized linear DNA is topologically constrained and cannot easily form supercoils, thereby limiting its transcriptional efficiency. Furthermore, the immobiliz-

Fig. 2 Fluorescence images and quantitative analysis of the Discosoma sp. red (DsRed) protein synthesized from immobilized circular DNA using a cell-free protein synthesis system at (A) 0, (B) 4, (C) 8, and (D) 16 h. (E) Quantitative comparison of DsRed yields at all time points. Fluorescence intensity was measured using ImageJ software. Statistical significance was determined using the *t*-test ($p < 0.01$). Error bars represent the standard deviation of three independent experiments ($n = 3$). Scale bar = 1 mm.

ation of one end of the DNA may restrict rotational freedom and local DNA relaxation, potentially reducing transcription efficiency compared to that of internally immobilized circular DNA triple-stranded structures. In cell-free protein synthesis, linear DNA is typically used as a template and is produced through PCR amplification. While linearizing circular DNA templates *via* restriction enzyme digestion facilitates a more thorough examination of topological relationships, incomplete digestion and potential inhomogeneity due to biotin labelling may hinder accurate evaluation. Therefore, this method was not used in the current study. This issue remains a subject for future research; however, the combination of these factors contributed to significantly enhanced mRNA and protein yields from circular DNA templates in this study.

To verify that the higher protein yield from the immobilized circular DNA was not simply due to a greater amount of DNA (*versus* the linear template), we performed a control experiment comparing protein synthesis from an immobilized circular DNA to that from an equivalent amount of free (non-immobilized) circular DNA in solution. In the latter case, the same circular plasmid was added to the cell-free reaction mixture without surface immobilization (*i.e.*, a standard solution-phase cell-free expression). The results showed very similar DsRed production under both conditions. Fluorescence images of *in situ*-immobilized circular DNA *vs.* free circular DNA in solution (Fig. 4A and B, respectively) had comparable intensities. Quantitative analysis (Fig. 4C) indicated that the DsRed yields were not significantly different (approximately 54.4 ng mm^{-2} for the free DNA reaction *vs.* 61.8 ng mm^{-2} for the immobilized DNA reaction). These results suggest that immobilizing circular DNA on the surface does not hinder its transcriptional or translational accessibility. In other words, the cell-free transcription/translation machinery can access and utilize surface-tethered circular DNA almost as effectively as DNA in a free solution. The immobilization method provides the benefits of template stabilization and reuse without compromising the protein expression efficiency.

3.3 Reusability of the immobilized circular DNA for protein synthesis

An important advantage of our DNA immobilization mehtod is the potential to reuse the same circular DNA-coated surface for multiple rounds of protein synthesis. We investigated this reusability by conducting seven consecutive cell-free synthesis cycles on a single DNA-immobilized substrate, with thorough washing between cycles. After each 8 hour reaction, the substrate was washed with water and a 1% Triton X-100 solution to remove residual reaction components (enzymes, expressed protein, *etc.*) while attempting to preserve the immobilized DNA. The substrate was then incubated with a fresh cell-free reaction mixture for the next cycle.

Fig. 5A shows fluorescence images of DsRed protein expressed on the substrate over seven sequential cycles. Strong fluorescence was observed in cycle 1, and visible fluorescence persisted through several cycles, diminishing with each successive round. The quantitative analysis of the DsRed expression yield per cycle is presented in Fig. 5B. The calculated amounts of DsRed synthesized in cycles 1–7 were approximately 61.8, 28.4, 19.4, 15.8, 11.0, 8.9, and 7.6 ng mm^{-2}, respectively. Notably, after the first cycle, the yield dropped by more than half and continued to decline in subsequent cycles. The decrease in protein synthesis output upon reuse is likely due to the gradual loss of immobilized circular DNA from the surface over multiple washes and reaction steps. Our method relies on triple-helix DNA interactions that are optimally stable under acidic conditions. However, cell-free protein synthesis reactions are carried out at near-neutral pH to maintain enzy-

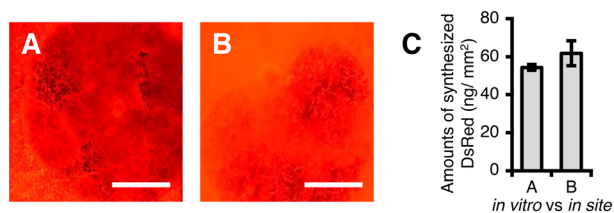**Fig. 4** Fluorescence images and quantitative analysis of DsRed protein synthesized using a cell-free system from (A) immobilized circular DNA (*in situ*) and (B) free circular DNA in solution (*in vitro*). The comparable fluorescence intensities observed in (A) and (B) indicate that immobilization did not impede protein synthesis. (C) Quantitative comparison of DsRed yields from (A) immobilized circular DNA and (B) free circular DNA. Fluorescence intensity was quantified using ImageJ software. Error bars represent the standard deviation of three independent experiments (*n* = 3). Scale bar = 1 mm.
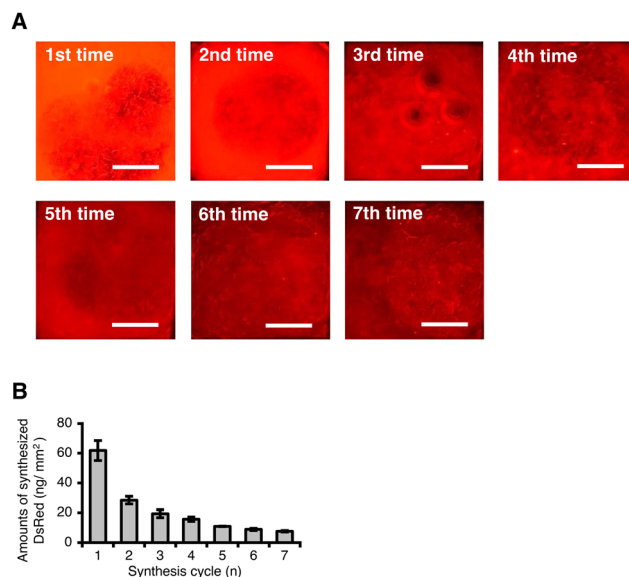
Fig. 5 (A) Fluorescence images of DsRed synthesized from immobilized circular DNA over seven consecutive protein synthesis cycles using a cell-free system. (B) Quantitative analysis of DsRed yield per cycle, with fluorescence intensities quantified using ImageJ software. Error bars represent the standard deviation of three independent experiments (*n* = 3). Scale bar = 1 mm.

matic activity.[41] Under these neutral conditions, the Hoogsteen bonds in the DNA triplex can partially dissociate,[42] potentially leading to the slow release of circular DNA from the surface with each cycle.

To verify that DNA loss was responsible for the decline in protein yield, we quantified the amount of circular DNA remaining on the substrate after each cycle (using SYBR Green I staining and image analysis; see Fig. S2). Indeed, the amount of immobilized DNA decreased by approximately 52% after the first synthesis cycle and continued to decrease with each subsequent cycle. This reduction in surface-bound DNA correlated well with the observed decrease in DsRed yield, supporting the conclusion that DNA dissociation was the primary factor diminishing protein synthesis over multiple uses. Despite the decrease in yield, it is noteworthy that even after four cycles, the amount of DsRed produced in that cycle ($\sim$15.8 ng mm^{-2} in cycle 4) was still higher than the initial yield from an immobilized linear DNA template ($\sim$12.7 ng mm^{-2} in the first and only cycle for linear DNA template). This highlights the superior performance of the circular DNA systems. The ability to produce detectable protein through seven cycles demonstrates the reusability of the immobilized circular DNA platform.

To further improve the reusability of DNA-functionalized surfaces, future studies should explore strategies to stabilize triple-helix interactions under neutral pH conditions. Possible approaches include chemically modifying the third strand (for example, using base analogs or backbone modifications that strengthen triplex formation at higher pH) or employing alternative triplex-forming chemistries that are inherently stable at physiological pH.[43] Additionally, covalent linkage strategies can be combined with the triplex approach to permanently tether circular DNA after initial targeting. By enhancing the stability of the immobilized DNA template, it should be possible to maintain high protein synthesis efficiency over many more reuse cycles, thereby increasing the practicality of this method for applications such as renewable biosensors and reusable protein microarray.

4. Conclusions

In this study, we successfully developed a novel method for immobilizing circular DNA *via* triple-helix formation, achieving significantly enhanced protein synthesis in cell-free systems compared to traditional methods using immobilized linear DNA. The triple-helix strategy allows for high-density, oriented immobilization of plasmid DNA on a surface, which, in turn, produces approximately 4.6 times more protein than the linear DNA template under identical conditions. The immobilized circular DNA also exhibited superior stability and could be reused over multiple synthesis cycles while maintaining a higher cumulative protein output than the linear DNA system. These remarkable improvements highlight the potential of immobilized circular DNA as a robust and efficient template for *in vitro* protein production.

This study demonstrates the potential application of triple-helix-mediated circular DNA immobilization in various fields. The enhanced stability, high yield, and reusability of the immobilized circular DNA make it an attractive platform for developing advanced biosensors, bioelectronic devices, and next-generation DNA/protein array technologies. By enabling the repeated use of DNA templates and boosting protein synthesis efficiency, our strategy contributes to the creation of high-performance biointerfaces and offers a new paradigm for on-surface genetic reactions in analytical and synthetic biology.

Author contributions

Shunsuke Takahashi: conceptualization, methodology, investigation, visualization, writing – original draft and review & editing Kazuki Hayashi: methodology, investigation, visualization Okada Jun: methodology, investigation Takashima Hibiki: methodology, investigation Nakata Koko: visualization Oshige Masahiko: conceptualization, supervision, writing – review & editing Katsura Shinji: conceptualization, supervision, writing – review & editing.

Conflicts of interest

The authors declare no conflicts of interest.

Data availability

The data supporting this article have been included in the main text and the supplementary information (SI). The supplemantary infomation includes detailed cloning schemes, plasmid maps and quantitative analyses of immobilized circular DNA before and after cell-free protein synthesis. Supplementary information is available. See DOI: https://doi.org/10.1039/d5an00995b.

Acknowledgements

References

1 A. Sassolas, B. D. Leca-Bouvier and L. J. Blum, *Chem. Rev.*, 2008, **108**, 109–139.
2 S. Cagnin, M. Caraballo, C. Guiducci, P. Martini, M. Ross, M. SantaAna, D. Danley, T. West and G. Lanfranchi, *Sensors*, 2009, **9**, 3122–3148.
3 F. Rusmini, Z. Zhong and J. Feijen, *Biomacromolecules*, 2007, **8**, 1775–1789.
4 H. M. Chan and H. W. Li, *Anal. Chem.*, 2011, **83**, 9370–9377.

5 J. C. Harper, R. Polsky, D. R. Wheeler, S. M. Dirk and S. M. Brozik, *Langmuir*, 2007, **23**, 8285–8287.

6 R. Hager, J. R. Burns, M. J. Grydlik, A. Halilovic, T. Haselgrübler, F. Schäffler and S. Howorka, *Small*, 2016, **12**, 2877–2884.

7 L. Sola, F. Damin and M. Chiari, *Anal. Chim. Acta*, 2019, **1047**, 188–196.

8 Y. Tu, G. Stolovitzky and U. Klein, *Proc. Natl. Acad. Sci. U. S. A.*, 2002, **99**, 14031–14036.

9 R. Benters, C. M. Niemeyer, D. Drutschmann, D. Blohm and D. Wöhrle, *Nucleic Acids Res.*, 2002, **30**, E10.

10 O. Stoevesandt, M. Taussig and M. He, *Expert Rev. Proteomics*, 2009, **6**, 145–157.

11 A. Lueking, Z. Konthur, H. Eickhoff, K. Büssow, H. Lehrach and D. Cahill, *Curr. Genomics*, 2001, **2**, 151–159.

12 G. A. Nascimento, E. V. Souza, D. S. Campos-Ferreira, M. S. Arruda, C. H. Castelletti, M. S. Wanderley, M. H. Ekert, D. Bruneska and J. L. Lima-Filho, *Biosens. Bioelectron.*, 2012, **38**, 61–66.

13 B. Saoudi, C. Despas, M. M. Chehimi, N. Jammul, M. Delamar, J. Bessière and A. Walcarius, *Sens. Actuators, B*, 2015, **62**, 35–42.

14 Q. Zheng, H. Wu, Z. Shen, W. Gao, Y. Yu, Y. Ma, W. Guang, Q. Guo, R. Yan and J. Wang, *Analyst*, 2015, **140**, 6660–6670.

15 F. Davis, M. A. Hughes, A. R. Cossins and S. P. Higson, *Anal. Chem.*, 2007, **79**, 1153–1157.

16 J. Wang, A. Shi, X. Fang, X. Han and Y. Zhang, *Microchim. Acta*, 2014, **181**, 935–940.

17 A. Benvidi, A. D. Firouzabadi, M. D. Tezerjani, S. Moshtaghiun, M. Mazloum-Ardakani and A. Ansarin, *J. Electroanal. Chem.*, 2015, **750**, 57–64.

18 X. Zhang, F. Gao, X. Cai, M. Zheng, F. Gao, S. Jiang and Q. Wang, *Mater. Sci. Eng., C*, 2013, **33**, 3851–3857.

19 K. Malecka, L. Michalczuk, H. Radecka and J. Radecki, *Sensors*, 2014, **14**, 18611–18624.

20 A. Erdem, P. Papakonstantinou, H. Murphy, M. McMullan, H. Karadeniz and S. Sharma, *Electroanalysis*, 2010, **22**, 611–617.

21 A. Dupont-Filliard, M. Billon, T. Livache and S. Guillerez, *Anal. Chim. Acta*, 2004, **515**, 271–277.

22 K. Wang, Y. Lei, G. X. Zhong, Y. J. Zheng, Z. L. Sun, H. P. Peng, W. Chen, A. L. Liu, Y. Z. Chen and X. H. Lin, *Bioelectron.*, 2015, **71**, 463–469.

23 A. Kowalczyk, A. M. Nowicka, R. Jurcakowski, P. Nieldzialkow, T. Ossowski and Z. Stojek, *Electroanalysis*, 2009, **22**, 49–59.

24 P. Botchan, J. Wang and H. Echols, *Proc. Natl. Acad. Sci. U. S. A.*, 1973, **70**, 3077–3081.

25 M. Gellert, K. Mizuuchi, M. O'dea and H. Nash, *Proc. Natl. Acad. Sci. U. S. A.*, 1976, **73**, 3872–3876.

26 K. Fox, T. Brown and D. Rusling, *Function, and Delivery*, Royal Society of Chemistry, Cambridge, U.K., 2018, pp 1–32.

27 B. Boehm, C. Whidborne, A. Button, T. Pukala and D. Huang, *Phys. Chem. Chem. Phys.*, 2018, **20**, 14013–14023.

28 M. Szabat, E. Kierzek and R. Kierzek, *Sci. Rep.*, 2018, **8**, 13023.

29 H. Zhou, B. J. Hintze, I. J. Kimsey, B. Sathyamoorthy, S. Yang, J. S. Richardson and H. M. Al-Hashimi, *Nucleic Acids Res.*, 2015, **43**, 3420–3433.

30 R. E. Campbell, O. Tour, A. E. Palmer, P. A. Steinbach, G. S. Baird, D. A. Zacharias and R. Y. Tsien, *Proc. Natl. Acad. Sci. U. S. A.*, 2002, **99**, 7877–7882.

31 N. C. Shaner, R. E. Campbell, P. A. Steinbach, B. N. Giepmans, A. E. Palmer and R. Y. Tsien, *Nat. Biotechnol.*, 2004, **22**, 1567–1572.

32 A. Arce, F. Guzman Chavez, C. Gandini, J. Puig, T. Matute, J. Haseloff, N. Dalchau, J. Molloy, K. Pardee and F. Federici, *Front. Bioeng. Biotechnol.*, 2021, **9**, 727584.

33 M. A. McSweeney and M. P. Styczynski, *Front. Bioeng. Biotechnol.*, 2021, **9**, 715328.

34 A. C. Batista, A. Levrier, P. Soudier, P. L. Voyvodic, T. Achmedov, T. Reif-Trauttmansdorff, A. DeVisch, M. Cohen-Gonsaud, J. L. Faulon, C. L. Beisel, J. Bonnet and M. Kushwaha, *ACS Synth. Biol.*, 2022, **11**, 732–746.

35 N. Michel-Reydellet, K. Woodrow and J. Swartz, *J. Mol. Microbiol. Biotechnol.*, 2005, **9**, 26–34.

36 J. H. Ahn, H. S. Chu, T. W. Kim, I. S. Oh, C. Y. Choi, G. H. Hahn, C. G. Park and D. M. Kim, *Biochem. Biophys. Res. Commun.*, 2005, **338**, 1346–1352.

37 K. Sitaraman, D. Esposito, G. Klarmann, S. F. Le Grice, J. L. Hartley and D. K. Chatterjee, *J. Biotechnol.*, 2004, **110**, 257–263.

38 R. Marshall, C. S. Maxwell, S. P. Collins, C. L. Beisel and V. Noireaux, *Biotechnol. Bioeng.*, 2017, **114**, 2137–2141.

39 T. A. Brooks and L. H. Hurley, *Nat. Rev. Cancer*, 2009, **9**, 849–861.

40 A. Travers and G. Muskhelishvili, *Nat. Rev. Microbiol.*, 2005, **3**, 157–169.

41 A. S. Karim, B. J. Rasor and M. C. Jewett, *Synth. Biol.*, 2019, **5**, ysz027.

42 Y. Hu, J. Ren, C. Lu and I. Willner, *Nano Lett.*, 2016, **16**, 4590–4594.

43 M. Pozza, A. Abdullrahman, C. J. Cardin, G. Gasser and J. Hall, *Chem. Sci.*, 2022, **13**, 10193–10215.